Kim *et al. Int J Concr Struct Mater* (2025) 19:12
https://doi.org/10.1186/s40069-024-00746-0

International Journal of Concrete Structures and Materials

RESEARCH

Open Access

Influence of Air Content on the Behavior of RC Beams Subjected to Freezing and Thawing

Sangwoo Kim[1], Yujeong Lee[2], Jinsup Kim[1*] and Dongyeop Han[2*]

Abstract

Research on concrete durability during prolonged use has been ongoing due to concrete's widespread use in construction. Freeze–thaw cycles exert a significant impact on concrete durability, especially in regions with harsh climates. While existing studies primarily focus on material aspects, research on the performance degradation of reinforced concrete (RC) structures is limited. This limitation is attributed to the inadequacy of current freeze–thaw testing standards for large structures like RC structures. Therefore, there is a need to propose freeze–thaw testing methods tailored for RC members. This study investigates the influence of air content and freeze–thaw cycles on the material and structural properties of RC beams, proposing a novel rapid freeze–thaw testing method for RC members. The study compares this new method (*N* test) with the conventional ASTM C666/C666M-15 rapid freeze–thaw testing procedure (*A* test), aiming to establish a correlation between the two experiments. Concrete mixtures with air content ranging from 0 to 9% underwent two types of freeze–thaw tests, followed by flexural testing of RC beams. The results were analyzed for air content, slump, compressive strength, mass loss, crack patterns, and failure modes, and they offer insights into the relationship between air entrainment, freeze–thaw resistance, and the structural behavior of RC under diverse environmental conditions.

Keywords RC beam, Air content, Freeze–thaw cycle, Bending behavior, Energy dissipation capacity

1 Introduction

Concrete, the most widely used structural material, is exposed to diverse environmental conditions. As a result of weather fluctuations, concrete structures endure varying temperature conditions, with the freeze–thaw cycle emerging as a well-known durability concern. This issue becomes particularly critical in regions with harsh climates, where water in concrete pores undergoes multiple freeze–thaw cycles (Chen et al., 2023; Kim et al., 2013; Mehta, 1991; Neville, 2001; Shi et al., 2012; Zhao et al., 2021). Since the accidental discovery of entrained air, air entrainer has become an indispensable admixture for concrete, conferring crucial durability against the freeze–thaw cycle. Following air entrainer's successful role in enhancing concrete durability in cold weather, numerous studies have investigated and reported on air entrainer and its influence on concrete properties (Cordon, 1967; Fülöp et al., 2022; Holan et al., 2020; Sun et al., 2023).

Extensive research has been conducted on air entrainers in concrete from a material perspective. However, many studies have predominantly focused on concrete as structural components. There is still insufficient research on the properties of concrete specifically as structural elements. Reinforced concrete (RC) members, such as RC beams or columns, consist of concrete and reinforcing bars. Changes in concrete properties due to various external and internal factors can

Journal information: ISSN 1976-0485 / eISSN 2234-1315

*Correspondence:
Jinsup Kim
jinsup.kim@gnu.ac.kr
Dongyeop Han
donald.dyhan@gnu.ac.kr
[1] Department of Civil Engineering, Gyeongsang National University, 501 Jinju-Daero, Jinju 52828, South Korea
[2] Departmentt. of Architectural Engineering, Gyeongsang National University, 501 Jinju-Daero, Jinju 52828, South Korea

significantly impact the performance of these structural members. Existing research on the freeze–thaw effect has predominantly concentrated on material aspects, such as the resistance and deformation characteristics of concrete in response to freeze–thaw. Some research has demonstrated that concrete degradation due to freeze–thaw significantly affects the performance of RC structures (Dahmani et al., 2007; Jiang et al., 2020; Luo et al., 2020; Rong et al., 2023a, 2023b; Wang et al., 2022; Yang et al., 2022; Yin et al., 2023; Zhang et al., 2021).

Rong et al. (2023a) model freeze–thaw damage in concrete while considering a non-uniform temperature field, and they examine its impact on structural performance. This study specifically proposes a method for modeling concrete damage in cases where the temperature distribution is non-uniform. In a related study, Rong et al. (2023b) experimentally investigate the seismic performance of RC beam–column connections after exposure to freeze–thaw cycles, evaluating how freeze–thaw damage affects structural seismic resistance. Zhang et al. (2021) develop a more refined model to simulate the lateral behavior of freeze–thaw damaged RC columns, incorporating the effects of reinforcement slip and shear. Collectively, these studies aim to provide a more precise understanding of how freeze–thaw damage impacts the performance of RC structures, particularly addressing the limitations of previous modeling techniques. Therefore, our research focuses on the freeze–thaw effects on structural elements such as RC beams. In addition, we propose a new freeze–thaw test (*N* test) method suitable for large-scale RC structures, aiming to overcome the limitations of existing standards. Furthermore, this study offers a comprehensive analysis by examining the impact of air content on the structural performance of RC members, extending beyond traditional material-focused research.

For a comprehensive assessment of the stability and durability of RC structures exposed to freeze–thaw conditions, it is essential to evaluate the performance of individual RC elements subjected to freeze–thaw exposure. Due to the porous nature of concrete, it readily absorbs moisture or humidity. When temperatures drop below the freezing point, the absorbed moisture freezes and expands, exerting increased pressure on surrounding air voids. This expansion leads to the generation of fine cracks in the internal structure of the concrete (Gong & Maekawa, 2018; Jang et al., 2009; Powers, 1945; Powers & Helmuth, 1953). Through these cracks, moisture penetration progresses from the concrete surface to the interior, contributing to complex deterioration mechanisms such as reinforcement corrosion and the promotion of concrete neutralization, resulting in a decline in overall durability.

The close connection between concrete as a material and RC members as structural elements underscores that concrete durability is closely linked to the performance of the RC member. Specifically, regarding durability under the freeze–thaw cycle, it is important to study how the degradation of concrete properties affects RC members. ASTM C666/C666M-15 (2016) provides a well-defined method for evaluating concrete durability under the freeze–thaw cycle. In addition, research, including work by Cordon (1967), widely recognizes the impact of entrained air content on concrete durability (see Fig. 1). However, due to the large size of structural members, conducting freeze–thaw tests for RC members is challenging, and the performance change of concrete should be separately analyzed or inferred for RC members.

The existing rapid freeze–thaw testing standards, primarily focused on material aspects, are deemed inadequate for conducting freeze–thaw experiments on large structures such as RC structures. Consequently, recent efforts by researchers have led to the proposal of new methods, such as the rapid air freezing–thawing test (Kim, 2023; Kim et al., 2020, 2021; Kwon et al., 2013, 2020; Rustamov et al., 2021). This method differs from the conventional approach in which the thawing process is carried out using air rather than water. This signifies a departure from the limitations of traditional freeze–thaw standards, expanding the scope to address the unique challenges posed by large-scale structures like RC members.

In this research, the objective is to validate the freeze–thaw evaluation method for structural members of RC beams by subjecting them to freeze–thaw cycles and assessing changes in concrete durability. To compare two different scaled evaluation methods, a material aspect analysis using concrete cylinder tests was also

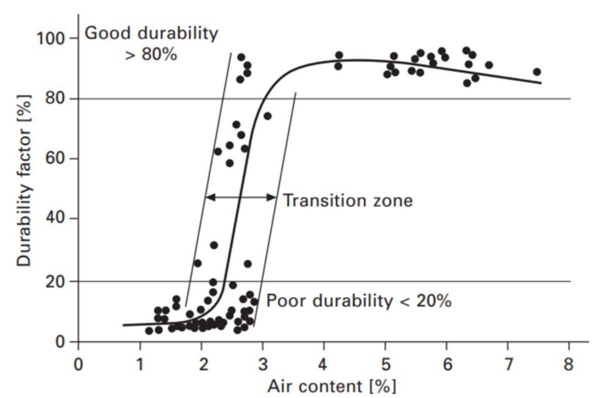

Fig. 1 Effect of air entrainment on the freeze–thaw durability of concrete when the freezing liquid is pure water (from Cordon, 1967))

executed and compared with the ASTM C666/C666M-15 (2016) standard, albeit with the same mix design but a different testing approach. Each sample of RC beams and cylinder specimens underwent freeze–thaw resistance performance evaluation through their respective test methods. Based on prior research by Cordon (Cordon, 1967), the influence of different air content in concrete on both RC beams and cylinder specimens were assessed. The experimental program involved different concrete mixtures, designated as M1, M2, and M3, each formulated with specific air content ranging from 0 to 9%. These mixtures were subjected to freeze–thaw tests, with subsequent analyses covering air content, slump, compressive strength, and mass loss. In addition, a series of RC beams, categorized into different groups based on air content and freeze–thaw cycles, were tested for flexural performance, crack patterns, and failure modes. The results of the research are expected to contribute to the field by providing a new perspective on structural test methods or actual scaled freeze–thaw tests and their reliability or correlation with the currently used materials-scaled freeze–thaw test results.

2 Experimental Program

2.1 Experimental Plan

The aim of the research was to compare freeze–thaw test results from both material and structural aspects. Therefore, the experiment was planned with two different series of tests sharing the same concrete mix design. The material test involved rapid freeze–thaw tests conducted on concrete in accordance with ASTM C666/C666M-15 standards (*A* test), commonly used in the research field. However, limitations in conducting experiments with large-sized RC specimens, as outlined in ASTM C666/C666M-15, led to the adoption of a new type of rapid freeze–thaw test for the structural evaluation (*N* test). Consequently, the experiments were designed to include a material perspective into the *N* test.

Fig. 2 illustrates the experimental timetable for this work. In the specimen fabrication phase, cylindrical concrete specimens were fabricated for material tests, while RC beam specimens were fabricated for structural tests. Evaluation of basic performance (air content test and slump test) was undertaken during the fabrication of the specimens. Subsequently, the curing process was carried out underwater.

In the material test, the *A* test were conducted for approximately 91 days, starting 28 days into the curing period. Simultaneously, the *N* test was performed for approximately 132 days, starting 124 days after the initial curing. The decision to extend the curing period to 124 days for the *N* test was based on findings from previous research (Kim et al., 2021), which demonstrated that the continued increase in concrete compressive strength after 28 days overlaps with the damage caused by freeze–thaw cycles, making it difficult to accurately measure the damage. Therefore, while the freeze–thaw experiments from a material perspective followed the ASTM-prescribed methods, the freeze–thaw test on the structural members was conducted after the enhancement effect of the concrete compressive strength had reached a certain point (The point when the increase of compressive strength is approximately 1 MPa). The compressive strength of concrete was checked at 3, 7, 14, 28, 42, 56, 70, 84, and 124 days during the curing process. Once the *N* test concluded, the compressive strength of the concrete was measured again. In the structural test, following a curing process of 124 days, RC beam

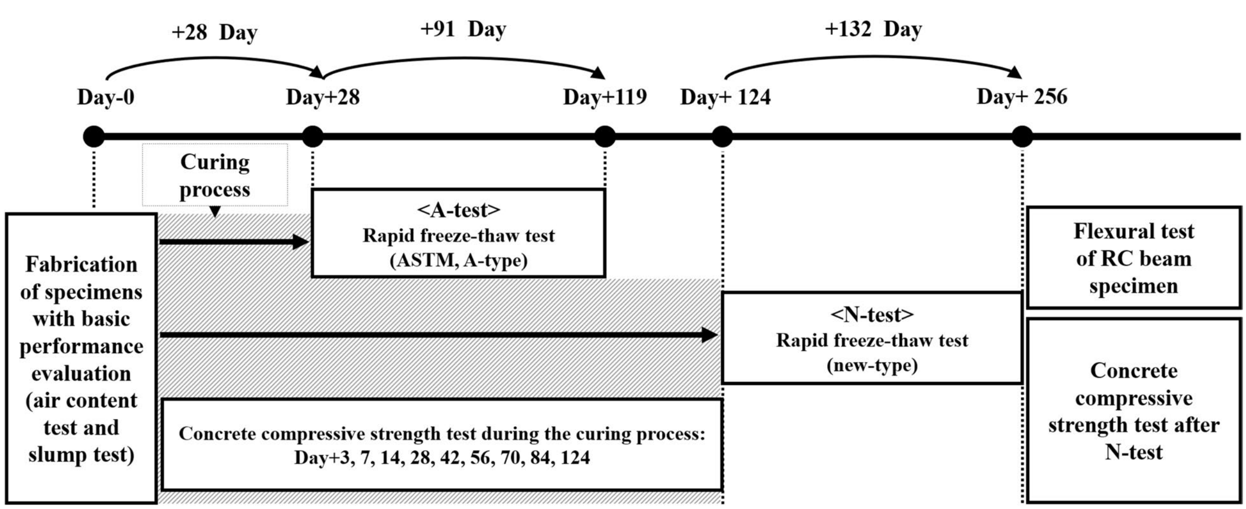

Fig. 2 Experimental timetable

Table 1 Physical and chemical properties of cement

Density (g/cm^3)	Blaine (cm^2/g)	Soundness (%)	Chemical component (%)				
			CaO	SiO_2	Fe_2O_3	SO_3	Al_2O_3
3.15	3.390	0.05	63.4	22.0	3.44	1.96	5.27

Table 2 Physical and chemical properties of superplasticizer (SP)

SP type	Phase	Color	Main component	Specific gravity	Solid content	pH
Generic type	Liquid	Brown	Polycarboxylate	1.048	20	5.4

Table 3 Physical properties of air entraining admixture (AE)

Phase	Color	Main component	Specific gravity	pH
Liquid	Light yellow	Surfactant	1.03	12

specimens were subjected to the N test, and flexural tests were conducted after the N test.

2.2 Materials Properties

2.2.1 Concrete

The concrete mix design was the same for both the material and structural tests. The cement used exhibited properties similar to type I ordinary Portland cement as per ASTM C150 (ASTM C150–07, 2022). Tap water was used as the concrete mixing water. Fine and coarse aggregates consisted of crushed aggregate obtained from South Korean aggregate manufacturers. These aggregates were of the same material typically used in ready-mixed concrete, and their properties complied with the standards outlined in KS F 2527 (KS F, 2527), the South Korean industrial standards for concrete aggregates, which closely align with ASTM C33 (ASTM C33/C33M-23, 2023). Chemical admixtures, specifically superplasticizers and air entrainers, were used, with these being commonly used products in the South Korean ready-mixed concrete industry. The properties of each material used are detailed in Tables 1, 2, and 3.

To assess the influence of different air content on concrete properties in both material and structural aspects, three different air content conditions were planned. According to ASTM C94 (2024), an appropriate range for air content in air-entrained concrete falls between 3.5% and 7.5%, with a suggested value of 4.5 ± 1.5% for moderate conditions with 25 mm nominal maximum sizes of aggregate. Hence, three different types of mixtures were used in this study, and these are listed in Table 4. Mixture M2 was initially set with a target air content range of 3.5–7.5%, while M1 contained 0–3.5% air content and M3 contained 7.5–10%. The quantities of air entrainer admixture were adjusted to achieve the desired air content within the concrete. Moreover, the proportions of fine and coarse aggregates were adjusted to align with the intended air content for each specific mixture.

2.2.2 Rebar

The longitudinal reinforcement used in the RC beam specimens consisted of deformed rebars with a diameter of 10 mm and a tensile yield stress grade of 400 MPa (SD400). The same type of rebars was also employed for the stirrups.

2.3 Specimen Preparation

2.3.1 Cylindrical Concrete Specimen

Eleven sets of cylindrical specimens (size: diameter 100 mm × height 200 mm) were prepared for each type of mixture to measure the compressive strength of concrete and an additional set of cylindrical concrete specimens of

Table 4 Concrete mix proportion

Mix No	Air content (%)	W/C	Cement (kg/m^3)	Water (kg/m^3)	FA (kg/m^3)	CA (kg/m^3)	AE (kg/m^3)	SP (kg/m^3)
M1	0–3.5	0.55	336.36	185	796.35	973.31	0	1.01
M2	3.5–7.5		336.36	185	740.11	904.58	0.5	1.01
M3	7.5–10		336.36	185	706.77	863.83	2.52	1.01

FA: fly ash, CA: Coarse aggregate

Table 5 Description of the cylindrical concrete specimens

Group name	Number of set	Description
C-1	9	Specimens used for compressive strength testing during water curing
C-2	1	Specimens tested after 300 cycles of the *A* test
C-3	1	Specimens stored in air during the *A* test and tested on the same date as Group 2
C-4	1	Specimens tested for compressive strength after the *N* test on RC beams

Table 6 Description of the RC beam specimens

Group name	Spec. ID	Mix No	Air content of concrete (%)	Number of freeze–thaw cycles
RC-1	N0-1	M1	0–2	0
	N0-2			
RC-2	F0-1			300
	F0-2			
RC-3	N5-1	M2	3–6	0
	N5-2			
RC-4	F5-1			300
	F5-2			
RC-5	N10-1	M3	7–9	0
	N10-2			
RC-6	F10-1			300
	F10-2			

the same size was created for *A* test (total 36 sets). Each set comprises three cylindrical concrete specimens.

The experiment was structured as follows: In Group 1(C-1), 9 sets of cylindrical specimens were used to assess changes in compressive strength during the curing process in water. In Group 2(C-2), 1 set of specimens was used to measure compressive strength after undergoing 300 cycles of the *A* test. In Group 3(C-3), 1 set of specimens was used to measure the compressive strength of concrete that was stored in air during the *A* test period and tested on the same date as Group 2(C-2). Finally, in Group 4(C-4), 1 set of specimens was used to evaluate the changes in compressive strength of concrete due to the *N* test applied to RC beams. The experimental plan for the cylindrical concrete specimens for each concrete mix is presented in Table 5.

2.3.2 RC Beam Specimen

For this experiment, 12 RC beam specimens were fabricated, as presented in Table 6. The test phase was divided into six groups based on the concrete's air content and freezing and thawing cycles. Groups 1 and 2 consisted of RC beam specimens with the M1 concrete mixture, while groups 3 and 4 consisted of RC beam specimens with the M2 concrete mixture. Groups 5 and 6 consisted of RC beam specimens with the M3 concrete mixture. Groups 1, 3, and 5 served as reference RC beam specimens for each design mixture, while Groups 2, 4, and 6 consisted of frozen–thawed RC beam specimens for each design mixture.

The total length of the RC beam was 1800 mm, and its cross section had a width of 100 mm and a height of 200 mm. The longitudinal reinforcement ratio was designed to be 0.35%. To analyze changes in the structural behavior within the pure flexural region of the RC beam between the top loading points, shear reinforcement was deliberately omitted, taking into account the effects of air entrainment and freeze–thaw conditions. All RC beams had the same reinforcement arrangement. The location of the strain gauge for longitudinal reinforcement (rebar) and the design of the RC beam are illustrated in Fig. 3.

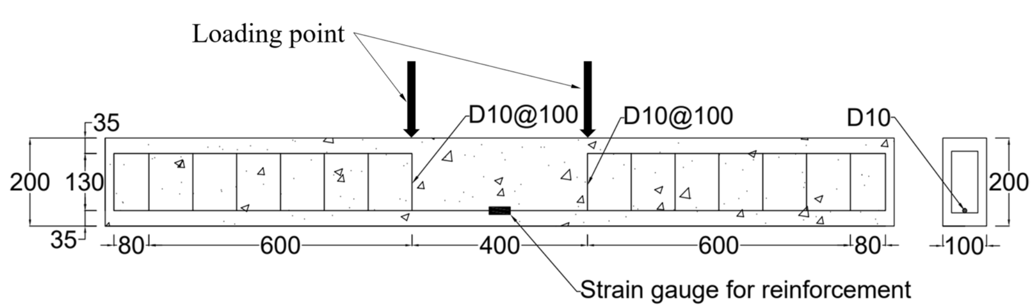

Fig. 3 Longitudinal and cross-sectional detail of an RC beam specimen (unit: mm)

2.4 Test Method

2.4.1 Basic Performance Evaluation Method (Fresh State Material Test)

Slump and air content were measured during the fresh state to assess the basic performance of concrete mixtures and mixing status. For the slump test, the ASTM C143 (2020) method was followed. The air content of the concrete mixtures was checked to ensure the target air content for each mixture. The air content of the fresh state concrete mixtures was measured using the ASTM C231 (2022) standard.

2.4.2 Concrete Compressive Strength Test

The concrete compressive strength test was conducted in accordance with KS F 2405 (2022). A 200-ton universal testing machine (UTM) was employed for the experiment. To measure the linear strain in the direction of the applied compressive force, linear variable differential transducers (LVDTs) were installed on both sides of the concrete specimen to measure the deformation. Fig. 4 shows the test setup for the concrete compressive strength.

Fig. 4 Concrete compressive strength test setup

2.4.3 Rapid Freezing and Thawing Test Method

(1) *A* test: Rapid freezing and thawing test (ASTM C666/C666M-15, A-type)

In accordance with ASTM C666/C666M-15 (2016), an A-type rapid freezing and thawing test was utilized to determine the durability index of each concrete mix. The rapid freeze–thaw testing machine completed approximately 3 cycles per day. During the testing period, non-destructive tests, including measurements of mass and relative dynamic modulus, were conducted every 30 cycles.

(2) *N* test: rapid freezing and thawing test in the air

For the freezing and thawing test on the RC beam specimen, a specially designed chamber for large-scale RC structures, as shown in Fig. 5, was used. Two cooling and heating machines were installed within the chamber, with one unit positioned on each side, left and right. The freeze–thaw experimental study followed the testing method outlined in the ASTM C666/C666M-15 (2016) standard specifications, with adjustments made to accommodate laboratory conditions. The novel aspect of the *N* test lies in the fact that, unlike conventional freezing–thawing methods, the thawing process is conducted using air. This offers the advantage of not requiring large amounts of water when conducting freezing–thawing experiments on large structural member units. However, it was ensured that the humidity within the chamber was continuously monitored by a hygrometer and maintained within the range of 60–70% throughout the freeze–thaw experiments.

The *N* test aimed to repetitively induce freezing and thawing temperatures, based on the temperature below the surface of concrete at a depth of 5 cm. The freezing–thawing temperatures were set to cycle between (4 ± 2)°C as the upper limit and (-18 ± 2)°C as the lower limit. To measure the temperature at a depth of 5 cm below the surface of the concrete, a concrete specimen with a diameter of 10 cm and a length of 40 cm was fabricated, with a temperature sensor positioned at the center. Although the temperature measurement was conducted in a cylindrical specimen, and the beam specimen has a rectangular cross section, which may lead to slight temperature differences due to the varying thermal capacity, we assumed the results were consistent for this study. The fabricated temperature-sensing specimen is depicted in Fig. 6. The temperature freeze–thaw cycle is presented in Fig. 7.

The experimental procedure for the *N* test begins with an initial freeze–thaw cycle conducted in an empty chamber to precondition the environment. Following this, the RC beam specimens are placed inside the chamber, and the freeze–thaw cycles are initiated based on the temperature measurements. The experiment

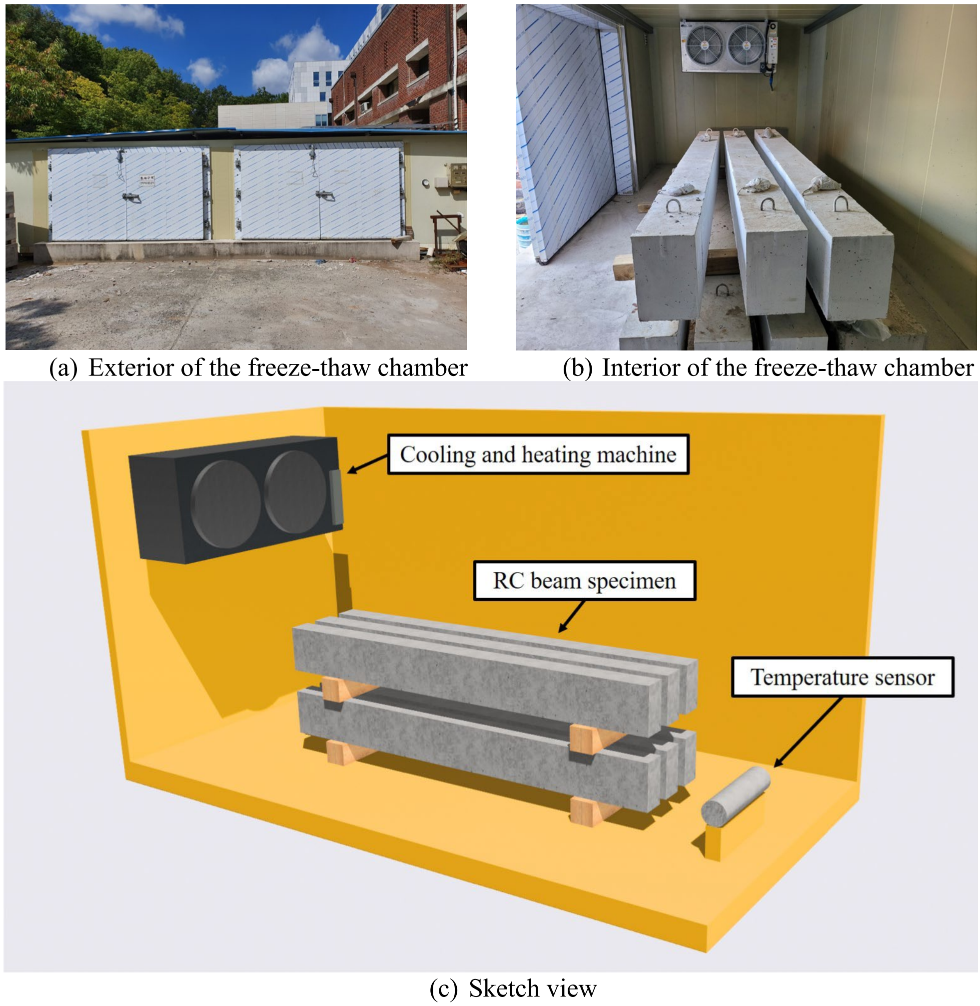

Fig. 5 Schematic drawing of the freeze–thaw chamber for structural members (*N* test)

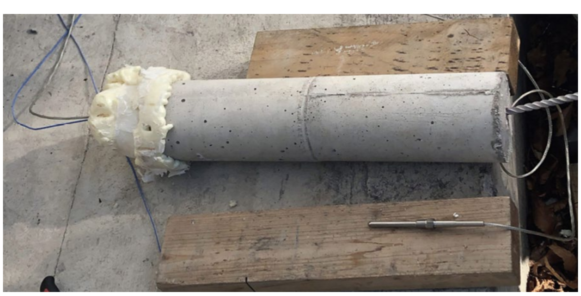

Fig. 6 Temperature-sensing method

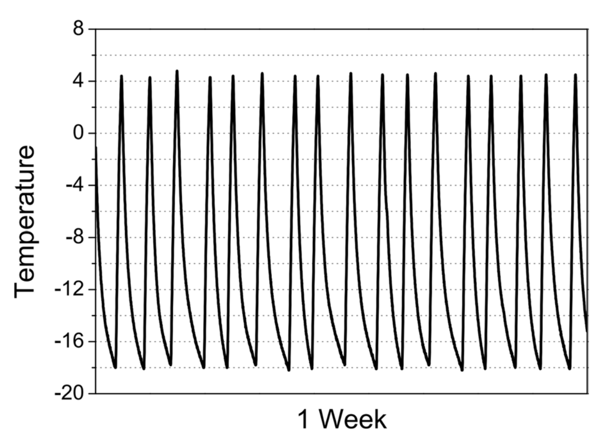

Fig. 7 Temperature scheme for the new rapid freeze–thaw test across 1 week

concludes once the target number of freeze–thaw cycles has been achieved. Temperature data over time were recorded using a thermometer with a temperature sensor inserted into a temperature-sensing specimen. The measurements indicated an average of 17–19 cycles per week. The non-destructive characterizing parameters, including mass and relative dynamic modulus, and the destructive compressive strength properties were measured at the beginning (0 cycles) and at the end (300 cycles) of the testing, respectively.

2.4.4 RC Beam Specimen Flexural Test

The flexural test setup used for testing the RC beam specimens is shown in Fig. 8. All test specimens were supported by two hinges, and a loading frame was placed at the mid-span above the specimen to distribute loads from the hydraulic jack to ensure a pure bending zone. The distance from the hinge and to the loading point was 500 mm. An LVDT was installed during the flexural testing to measure mid-span deflection. All test specimens were subjected to flexural testing following a displacement-controlled loading protocol at a 1 mm/min speed.

3 Test Results and Discussion

3.1 Basic Performance of Concrete

In the context of evaluating the material and structural aspects after exposure to freeze–thaw cycles, the air content in the unset concrete emerged as a crucial factor. Utilizing the ASTM C231 (2022) pressure method, a Washington-type concrete air meter was employed to determine the air content within the concrete, as depicted in Fig. 9. For mixture M2, the measured air content was 4.1%, while for M1 and M3, the respective measurements were 1.1% and 8.7%. These results confirm that the actual air content is closely aligned with the target values, indicating that the concrete mixtures were appropriately designed and the air content was effectively controlled during the vibrating process.

By measuring the concrete fluidity, the adequacy of concrete mixtures was assessed. The results for different air content concrete are presented in Fig. 10. As observed in the figure, the slump exhibited a distribution ranging from 60 to 150 mm. This distribution, falling within the specified air content range of 185 kg/m^3 for the M2 mixture, suggests an appropriate level of fluidity. In other words, no peculiarities in terms of fluidity were identified in the concrete mixture. In the case of the M1 mixture with very low air content, the fluidity was significantly lower. This was attributed to the adverse impact on fluidity caused by the increased aggregate volume resulting from the removal of air during the

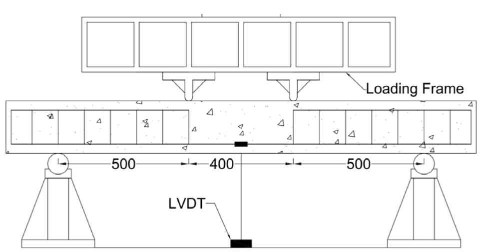

(A) Illustration of the flexural test setup (unit: mm)

(B) Photo of the flexural test setup

Fig. 8 Test setup of the flexural test for RC beam specimens

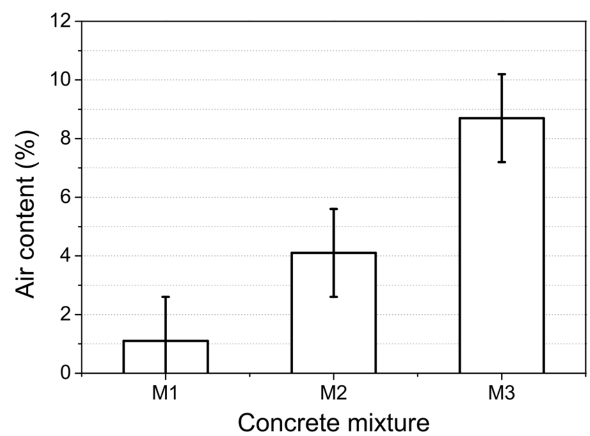

Fig. 9 Air content of concrete

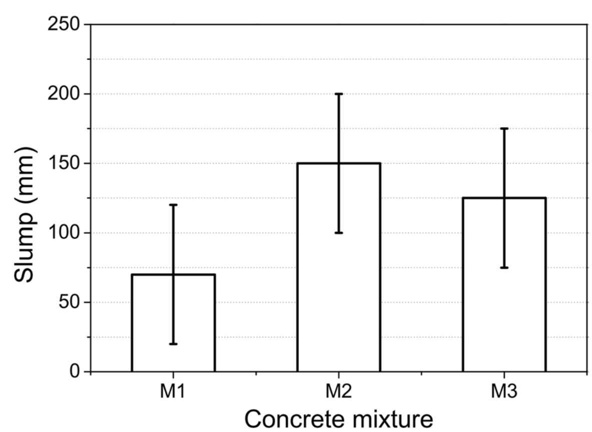

Fig. 10 Concrete slump amounts

mixing process (Maiti et al., 2006; Salem & Pandey, 2015). Conversely, for the M3 mixture with very high air content, the slump of 125 mm showed a slight decrease in fluidity compared to the M2 mixture. However, this was deemed to be within the margin of error, indicating a similar level of fluidity. It appears that excessive air content does not continuously affect the mixture (Shin et al., 2019).

3.2 Concrete Compressive Strength

3.2.1 Checking Compressive Strength During the Curing Process

Fig. 11a shows the compressive strength at 3, 7, and 28 days, while Fig. 11b depicts the concrete compressive strength measured throughout the curing period. As observed in Fig. 11a, M2, with an appropriate amount of air content, exhibited strength levels consistent with the planned water–cement ratio for the concrete in the study. In contrast, M1, with very low air content, showed the highest strength, while M3, with very high air content, exhibited the lowest strength. This can be attributed to the low air content in M1, which influenced the densification of the interior during the specimen fabrication process, reducing voids and resulting in higher strength compared to other mixtures. In the case of M3, with very high air content, the increased porosity within the concrete contributes to the observed strength reduction.

Continuous strength measurements were taken over 28 days to minimize the concrete's compressive strength increase during the curing process. These measurements revealed a limited increase in compressive strength after 56 days of curing. Consequently, the curing process was halted on the 124th day. The concrete reached its highest compressive strength after 124 days of curing, measuring 50.33 MPa for M1, 25.99 MPa for M2, and 17.71 MPa for M3, respectively.

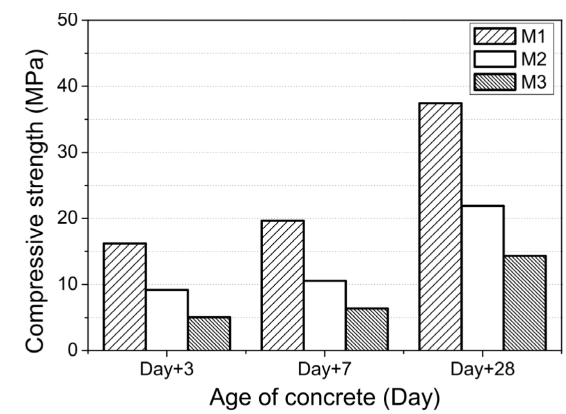

(a)

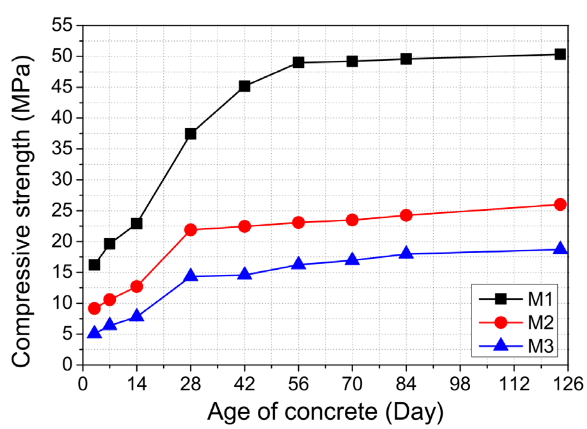

(b)

Fig. 11 Compressive strength of concrete during the curing process

3.2.2 Compressive Strength due to N Test

The change in compressive strength for each type of mixture with *N* test is shown in Fig. 12. For each type of mixture, three sets of cylindrical concrete specimens were manufactured to assess the compressive strength under freeze–thaw conditions. The first set was tested at the beginning of the freeze–thaw experiment (0 cycles). The second set underwent testing after being exposed to 300 freeze–thaw (FT) cycles, whereas the third set was cured in air (AC) at the commencement of the freeze–thaw experiment and tested on the same date as the second set.

The compressive strength of the M1 concrete mix was initially measured at 50.33 MPa before the onset of freeze–thaw cycles. Following the freeze–thaw cycles, the compressive strength decreased to 49.36 MPa. Subsequently, after air drying during the freeze–thaw period, the compressive strength was determined to

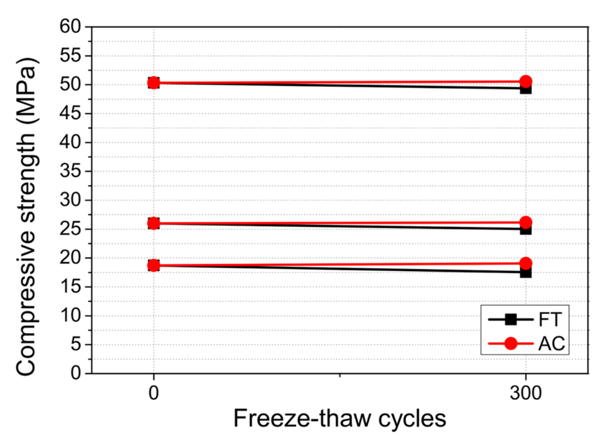

Fig. 12 Influence of freeze–thaw cycles on the compressive strength depending on curing conditions

be 50.66 MPa. As a result, it was observed that the compressive strength exhibited no significant changes with the initiation and progression of freeze–thaw cycles, and there was an approximate 2.3% reduction in compressive strength attributed to the effects of freeze–thaw.

In the case of the M2 concrete mix, the compressive strength was initially measured at 25.99 MPa before the commencement of freeze–thaw cycles. Following freeze–thaw cycles, the compressive strength decreased to 25.03 MPa. Subsequently, after air drying during the freeze–thaw period, the compressive strength was also measured at 26.17 MPa. Consequently, it was observed that with the initiation and progression of freeze–thaw cycles, the compressive strength decreased by approximately 1.14 MPa, and there was a slight decrease of about 1.14% in compressive strength attributed to freeze–thaw effects.

For the M3 concrete mix, the compressive strength measured 18.71 MPa before initiating freeze–thaw cycles, whereas the compressive strength decreased to 17.54 MPa after these cycles. The compressive strength following air drying during the freeze–thaw period was also measured at 19.08 MPa. Consequently, it was observed that the compressive strength remained relatively stable with the onset and progression of freeze–thaw cycles, resulting in an approximate 8.1% decrease in compressive strength due to the effects of freeze–thaw.

In a comprehensive analysis, the M1 mix demonstrated the highest resistance to freeze–thaw cycles, resulting in the lowest rate of compressive strength reduction. The M2 mix exhibited a slightly higher reduction rate compared to M1, but still maintained stable performance. In contrast, the M3 mix showed the highest rate of compressive strength reduction, indicating the greatest vulnerability to freeze–thaw cycles. This is attributed to the concurrent decrease in compressive strength as the air content increases.

3.3 Durability After Rapid Freezing and Thawing Test

3.3.1 Results of A Test (ASTM C666/C666M-15, A-type)

(1) Relative dynamic modulus

The results of measuring the relative dynamic modulus of concrete, according to variations in the A-type of freeze–thaw cycles, are presented in Fig. 13. It was observed that as the freeze–thaw cycles increased, the dynamic modulus of elasticity of all specimens decreased due to damage caused by freeze–thaw. In particular, the dynamic modulus of elasticity for M3, which had the highest air content, showed a significant decrease of 7.96% compared to M2, yielding the lowest result.

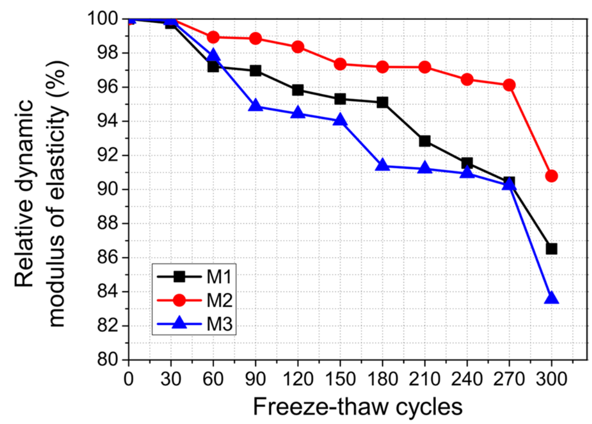

Fig. 13 Influence of freeze–thaw cycles (*A* test) on relative dynamic modulus of elasticity depending on air content

On the other hand, M2 exhibited the highest dynamic modulus of elasticity, indicating the least damage from freeze–thaw. This aligns with previous research findings, attributing the reduced freeze–thaw susceptibility to the inclusion of an appropriate amount of entrained air, approximately 3–6% within the concrete (Oh et al., 1993; Park et al., 2020; Shang et al., 2009).

Despite having the highest compressive strength, M1 is presumed to have suffered more damage from freeze–thaw due to significantly lower air content compared to M2. Conversely, M3 experienced a notable degradation in freeze–thaw resistance due to an excessive amount of entrained air within the concrete. In summary, the results of the A-type rapid freeze–thaw test are consistent with previous research, revealing that both insufficient and excessive air content can undermine freeze–thaw resistance. Therefore, these results are aligned with prior studies.

(2) Durability index

The durability index was computed using Eq. (1), where D.I. represents the durability index, R denotes the relative dynamic modulus, and FTC signifies the freeze–thaw cycles. The durability index was measured every 30 cycles during A test, ranging from 0 to 300 cycles:

$$\text{D.I.} = \frac{R \times \text{FTC}}{300} \tag{1}$$

Examining the durability index presented in Fig. 14, it is evident that up to 150 freeze–thaw cycles, there is no significant difference in the durability index among M1, M2, and M3. However, after 180 freeze–thaw cycles, the range of changes in the durability index becomes more pronounced. Comparing the durability index after

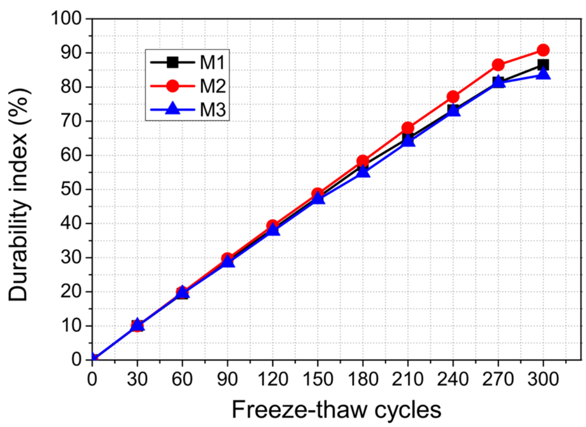

Fig. 14 Relationship between durability index and freeze–thaw cycles (A-type)

completing 300 freeze–thaw cycles, it is observed that the mixture with the optimal air content, M2, exhibits the highest durability index, while M3, with the highest air content, shows the lowest durability index. Similar to the results of the relative dynamic modulus measurements, this suggests that M3, with the highest air content, is vulnerable to freeze–thaw damage due to excessive internal porosity in the concrete specimens.

Furthermore, M1, with the least air content, demonstrates a relatively low porosity, allowing for densification within the specimen. While M1 exhibits a higher durability index compared to M3, it falls short of achieving the air content necessary to withstand freeze–thaw damage. Consequently, M1 is found to have a diminished freeze–thaw resistance compared to M2, which falls within the optimal air content range.

(3) Mass loss

For the *A* test specimens, the mass loss was measured in the surface-dry state at a temperature of 6 ± 3 ℃ immediately after being removed from the chamber. Mass loss was calculated by the following equation:

$$\Delta W_n = \frac{W_0 - W_n}{W_0} \times 100\% \quad (2)$$

where ΔW_n is the mass loss rate after the freeze–thaw cycles, W_0 is the initial mass, and W_n is the residual mass after n freeze–thaw cycles. The results of measuring the Mass loss of concrete according to variations in the freeze–thaw cycle count are presented in Table 7, and Fig. 15 shows the relationship between mass loss rate and freeze–thaw cycles.

As the number of freeze–thaw cycles increased, the mass of specimens for M1, M2, and M3 decreased. Examining the mass loss rate after 300 freeze–thaw cycles, it is evident that M2, with an optimal air content, exhibited the lowest mass loss rate, while M3, with the highest air content, showed the highest mass loss rate. The trend in mass loss rate with increasing freeze–thaw cycles aligns with results observed in relative dynamic modulus and durability index measurements. This indicates that both insufficient and excessive air content in concrete can influence freeze–thaw resistance, highlighting the effectiveness of maintaining an optimal air content range for securing freeze–thaw resistance.

3.3.2 Results of N Test

(1) Relative dynamic modulus

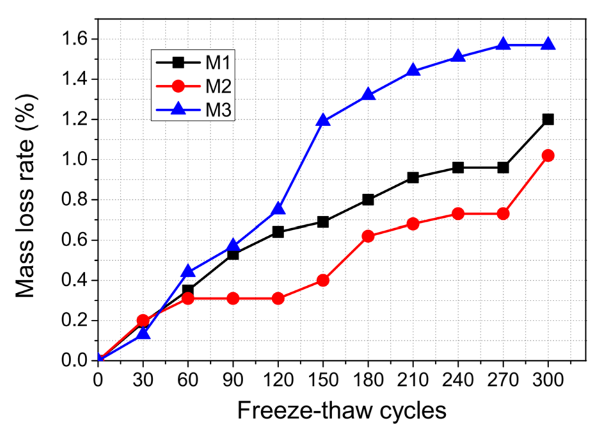

Fig. 15 Relationship between mass loss rate and freeze–thaw cycles (*A* test)

Table 7 Mass loss rate after rapid freeze–thaw cycles in water (Unit: %)

Mix No	Freeze–thaw cycles										
	0	30	60	90	120	150	180	210	240	270	300
M1	0.00	0.19	0.35	0.53	0.64	0.69	0.80	0.91	0.96	0.96	1.20
M2	0.00	0.20	0.31	0.31	0.31	0.40	0.34	0.40	0.48	0.68	0.60
M3	0.00	0.13	0.44	0.57	0.75	1.19	1.32	1.44	1.51	1.57	1.57

The results of measuring the relative dynamic modulus of concrete according to variations in the *N* test are presented in Fig. 16. An increase in the freeze–thaw cycles has been indicative of a decrease in the relative dynamic modulus. Concrete mixture M2, characterized by an optimal air void content, exhibited the highest relative dynamic modulus, while concrete mixture M1, with the lowest air void content, demonstrated the lowest relative dynamic modulus.

(2) Durability index

Fig.17 presents the durability index assessed at 100-cycle intervals throughout the *N* test process, covering a range from 0 to 300 cycles. As the number of freezing–thawing cycles increased, there was an observed increase in the durability index. Up to 100 cycles, there was no significant difference in the durability index among the mixtures. However, starting from 200 cycles, the durability index exhibited an increasing discrepancy between each mixture. Ultimately, at 300 cycles, the M2 mixture with the optimal air void content demonstrated the highest durability index, while the M1 mixture exhibited the lowest.

(3) Mass loss

For the *N* test specimens, the mass was measured in the dry state at the temperature of 6 ± 3 °C (same temperature with A-type specimen) immediately after being removed from the chamber. Table 8 presents the mass loss rates of each concrete mixture in response to the freezing–thawing cycles. The results revealed negligible mass loss rates attributed to the freezing–thawing, irrespective of the mixture composition (i.e., regardless of air void content).

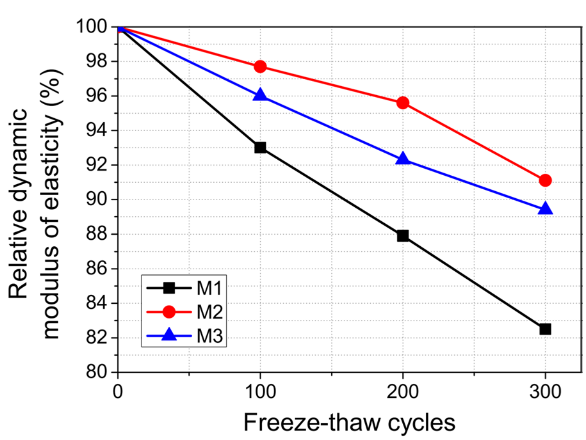

Fig. 16 Influence of freeze–thaw cycles (new type) on relative dynamic modulus of elasticity depending on air content

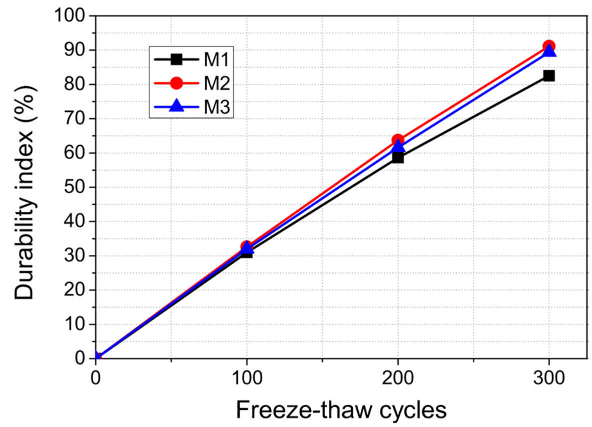

Fig. 17 Relationship between durability index and freeze–thaw cycles (*N* test)

3.3.3 Discussion of the Two Types of Rapid Freezing and Thawing Tests

The freeze–thaw resistance of the M2 mixture, which contained an appropriate amount of air, was found to be the highest among the two freeze–thaw methods tested. For the *A* test, the relative dynamic modulus of elasticity and durability index of the M1 mixture, with insufficient air content, increased by 4.71% compared to the M2 mixture. The mass loss rate of the M1 mixture increased by 17.65% compared to that of the M2 mixture. For the M3 mixture, which had excessive air content, the relative dynamic modulus of elasticity and durability index decreased by 7.96% compared to the M2 mixture, while the mass loss rate increased by 53.92% compared to the M2 mixture.

In the case of the *N* test, the relative dynamic modulus of elasticity and durability index of M1, with insufficient air content, decreased by 9.44% compared to M2, while M3 with excessive air content decreased by 1.87% compared to M2. In terms of mass loss rate, there was no significant difference based on air content for the new type of rapid freeze–thaw.

Table 8 Mass loss rates of each concrete mixture

Mix No	Freeze–thaw cycles			
	0	100	200	300
M1	0.00	0.01	0.02	0.02
M2	0.00	0.01	0.02	0.02
M3	0.00	0.01	0.02	0.02

These results can also be considered in the context of ASTM C666/C666M-15, where the freezing and thawing actions underwater (Type A) are perceived to be much harsher than in air conditions. Furthermore, underwater freezing and thawing actions are believed to have a deeper impact on concrete by interacting with moisture in the capillary pores.

The experimental results in this study suggest that an appropriate air content in concrete enhances freeze–thaw resistance. However, both insufficient and excessive air content can diminish freeze–thaw resistance. This observation holds true for both *A* test and the *N* test applied to structures. In the *A* test, significant damage due to freeze–thaw was observed in the order of M3, M1, and M2. Conversely, in the *N* test, significant damage due to freeze–thaw was measured in the order of M1, M3, and M2. This observation aligns with the finding that the concrete mix (M2) within the appropriate air content range experienced the least damage, as also observed in the previous results of Cordon (1967).

3.4 Flexural Test of the RC Beam Specimens

3.4.1 Crack Patterns and Failure Modes

The final failure modes for all RC beam specimens are shown in Fig. 18. As expected, flexural failure, accompanied by steel yielding followed by concrete crushing, is the observed failure mechanism for all RC beam specimens. Initial vertical cracks originated from

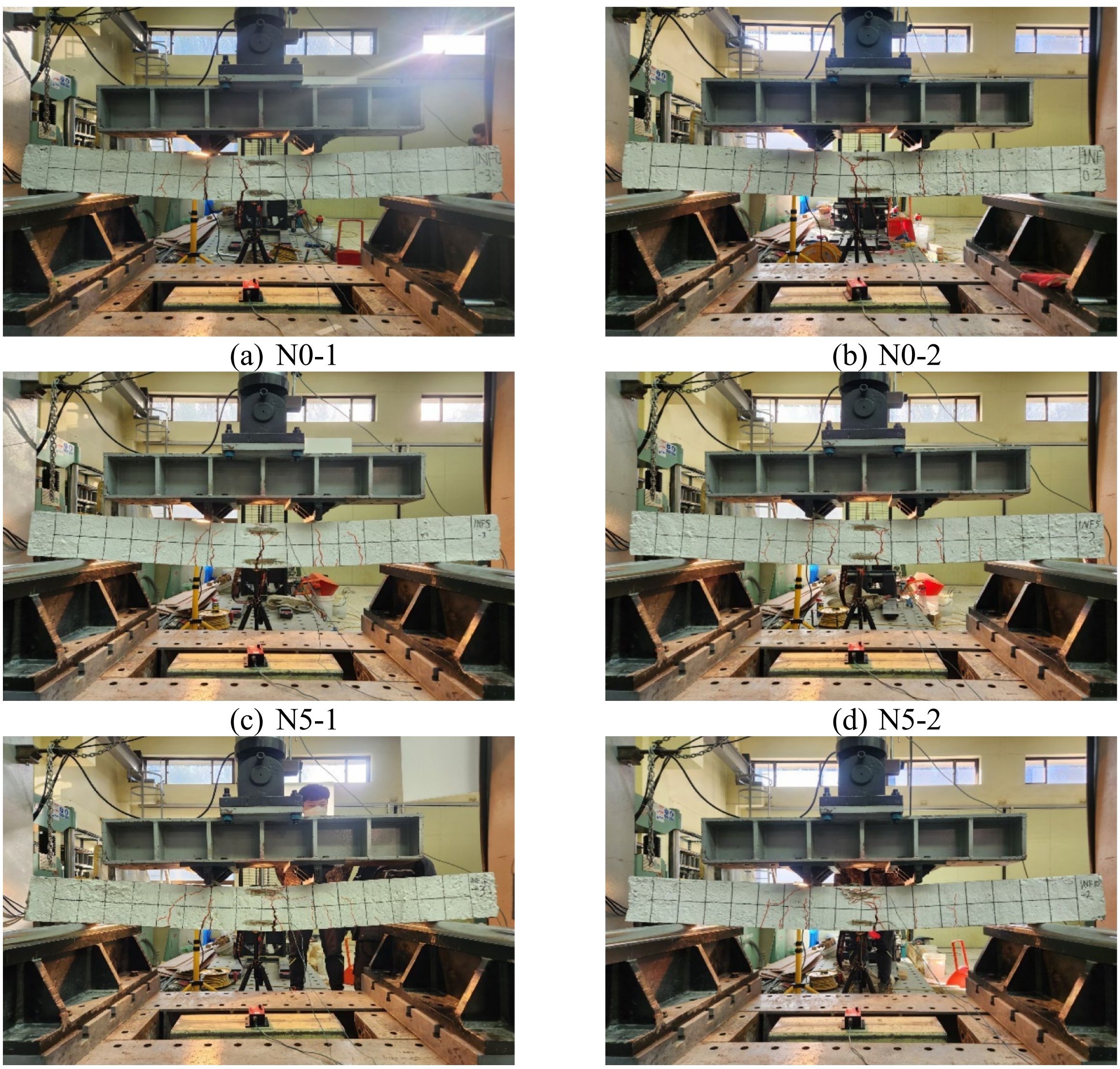

(a) N0-1 (b) N0-2

(c) N5-1 (d) N5-2

(e) N10-1 (f) N10-2

Fig. 18 Final failure modes

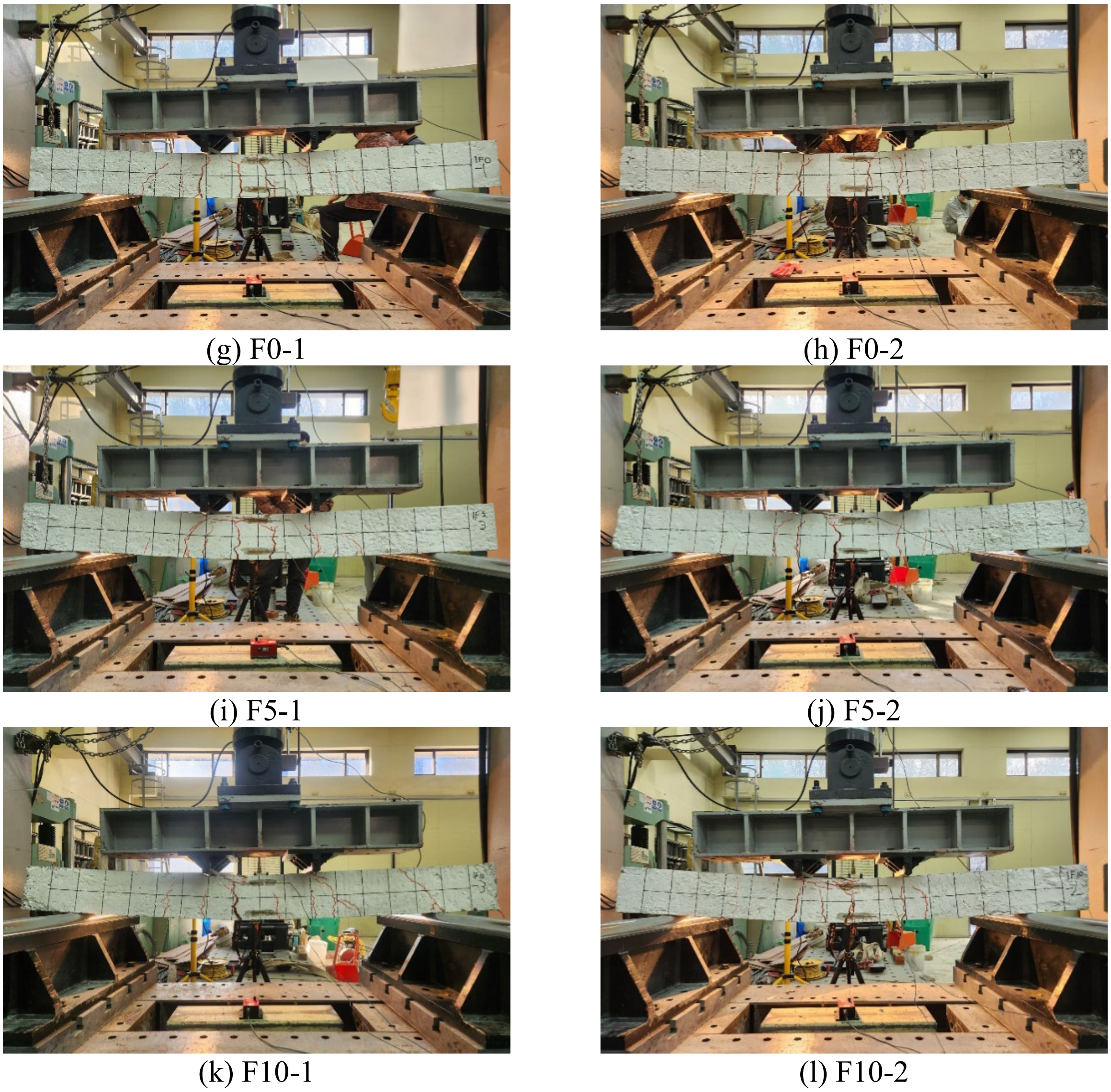

Fig. 18 continued

the tensile region and gradually extended to the top as the loading displacement increased. With additional load displacement, the development of flexural cracks persisted, culminating in a final failure mode attributed to compressive failure at the top surface of the pure bending region.

3.4.2 Load–Deflection Relationship

The load against the mid-span deflection curve for all RC beam specimens is shown in Fig. 19. Moreover, Table 9 presents the data obtained for each RC beam specimen in terms of cracking load (P_{cr}), yield load (P_y), and their respective deflections Δ_{cr}, Δ_y.

For groups 1, 3, and 5, which did not undergo freeze–thaw cycles, it was observed that the initial flexural cracking load (P_{cr}) tended to decrease as the air content of the concrete increased. In addition, there was an increasing trend in cracking deflection (Δ_{cr}) when the first flexural crack was measured. Therefore, it is inferred that as the concrete's air content increases, the cracking deflection increase suggests a decrease in the bond strength between the reinforcement and the concrete within the RC beam specimen.

The cracking load (P_{cr}) and respective deflections Δ_{cr} of the groups subjected to freeze–thaw experiments (groups 2, 4, 6) exhibited a similar trend to that of groups 1, 3, 5, which did not undergo freeze–thaw

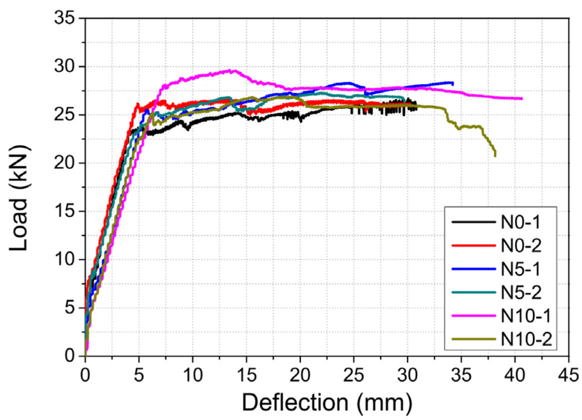

(a) Not subjected to freeze-thaw cycles (N0, N5 and N10)

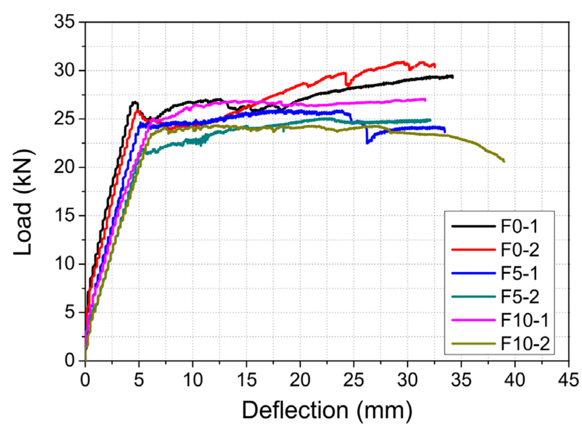

(b) Subjected to freeze-thaw cycles (F0, F5 and F10)

Fig. 19 Load–deflection relationships of the tested RC beams

cycles. This is attributed to minimal damage to the compressive strength of concrete due to freeze–thaw, with all concrete exhibiting resistance to freeze–thaw. Therefore, an increase in air content leads to a decrease in cracking load and an increase in cracking deflection, yet the impact of freeze–thaw on the cracking load of the RC beams is considered relatively minimal.

The yield load (P_y) and yield deflection (Δ_y) demonstrate an increasing trend with the rise in air content, attributed to the occurrence of larger deflection and, consequently, greater loads under the same applied displacement. The larger deflection under the same applied displacement is considered to result from a decrease in the bond strength between concrete and reinforcement due to the increased air content. Moreover, even in freeze–thaw conditions, the yield load (P_y) and yield deflection (Δ_y) values exhibited very similar figures. Groups 1 and 2 increased by 1.78 MPa, 3 and 4 decreased by 1.59 MPa, and 5 and 6 decreased by 2.24 MPa. Consequently, it is concluded that the impact of freeze–thaw on the yield load (P_y) and respective deflections Δ_y of the RC beams is considered relatively minimal.

3.4.3 Elastic Stiffness and Energy Absorption Capacity

The elastic stiffness and energy absorption capacity are presented in Table 10. The elastic stiffness was calculated as the slope of the linear portion in the load–deflection curve, while the energy absorption capacity was defined as the area under the load–deflection curve up to the yield load.

The increase in the air content of concrete results in a decrease in the elastic stiffness of RC beam specimens. This phenomenon is judged to stem from the reduction in concrete strength as the air content increases,

Table 9 RC beam specimen test results

Group name	Spec ID	P_{cr} (kN)		Δ_{cr} (mm)		P_y (kN)		Δ_y (mm)	
		Each	Ave	Each	Ave	Each	Ave	Each	Ave
RC-1	N0-1	7.51	8.26	0.57	0.64	22.98	24.46	4.05	4.51
	N0-2	9.00		0.71		25.95		4.96	
RC-2	F0-1	8.31	9.14	0.47	0.78	26.66	26.24	4.44	4.68
	F0-2	9.97		1.09		25.81		4.91	
RC-3	N5-1	7.36	7.97	0.95	0.83	25.39	24.67	5.87	5.67
	N5-2	8.57		0.72		23.96		5.47	
RC-4	F5-1	5.70	4.80	0.67	0.53	24.27	23.08	5.42	5.41
	F5-2	3.90		0.38		21.89		5.40	
RC-5	N10-1	6.85	6.68	1.14	1.14	27.80	26.46	7.46	6.89
	N10-2	6.51		1.14		25.12		6.33	
RC-6	F10-1	7.70	6.52	1.14	1.04	24.92	24.22	6.41	6.38
	F10-2	5.35		0.94		23.52		6.35	

Table 10 Elastic stiffness and energy absorption capacity of the RC beam specimens

Group Name	Spec ID	Elastic stiffness (kN/mm)		Energy absorption capacity (kN·mm)	
		Each	Ave	Each	Ave
RC-1	N0-1	4.53	4.35	78.16	80.25
	N0-2	4.17		82.33	
RC-2	F0-1	4.86	4.77	73.56	76.19
	F0-2	4.67		78.81	
RC-3	N5-1	3.93	3.86	87.04	86.95
	N5-2	3.79		86.85	
RC-4	F5-1	4.35	4.02	79.18	72.58
	F5-2	3.69		65.98	
RC-5	N10-1	3.70	3.86	120.10	107.40
	N10-2	4.02		94.70	
RC-6	F10-1	3.53	3.56	97.20	91.18
	F10-2	3.58		85.16	

leading to the consequent impairment of the bonding capacity between the reinforcement and concrete. On the other hand, no significant correlation was observed between freeze–thaw and elastic stiffness. This finding suggests that the concrete's sufficient resistance to freeze–thaw minimizes its impact on the elastic stiffness of RC beams.

The energy absorption capacity shows an increasing trend with the increase in air content. This is attributed to the simultaneous increase in yield load and yield deflection of the RC beam due to the elevated air content. N5 and N10 exhibited significantly higher values, 6.7 kN mm and 27.15 kN mm, respectively, compared to N0. The energy absorption capacity of RC beams showed a decreasing trend with exposure to freeze–thaw cycles. This is attributed to the weakening of concrete strength due to freeze–thaw, leading to increased stress distribution on the reinforcement and a subsequent decrease in bonding capacity between the concrete and the reinforcement. The energy absorption capacity of the RC beams subjected to freeze–thaw cycles was lowest in RC-4, at 72.58 kN mm. In contrast, RC-6 showed the highest capacity among the tested groups, with 91.18 kN mm. This result can be attributed to the high compressive strength of RC-2's concrete, which likely limited deformation due to bending, leading to a greater energy absorption capacity than RC-4. In addition, RC-6's superior energy absorption is likely due to its high air content, which may have allowed for more effective load distribution and absorption.

4 Conclusion

This study introduces a novel rapid freeze–thaw testing method for RC members and compares it with the ASTM C666/C666M-15 standard. The results provide insights into the relationship between air content, freeze–thaw resistance, and structural behaviors. Conclusions drawn from the experimental results are as follows:

(1) Concrete mix with an appropriate air content (M2) exhibited the highest freeze–thaw resistance, consistently performing better in both the traditional freeze–thaw test (*A* test) and the new type of freeze–thaw test (*N* test).
(2) Cracking load of RC beam tended to decrease with increasing air content for groups not subjected to freeze–thaw cycles, indicating a decrease in the bond strength between reinforcement and concrete. The cracking load and corresponding deflection, as well as the yield load and yield deflection of the groups subjected to freeze–thaw cycles (groups 2, 4, 6), exhibited similar trends to those of groups 1, 3, and 5, which were not exposed to freeze–thaw cycles. In addition, the failure mode was consistently observed as flexural failure across all groups.
(3) The increase in air content led to a decrease in the elastic stiffness of RC beams, attributed to a reduction in concrete strength and impairment of bonding capacity. Energy absorption capacity increased with higher air content, correlating with increased yield load and yield deflection. Energy absorption capacity decreased with exposure to freeze–thaw cycles due to the weakening of concrete strength.
(4) In this study, the adjustment of the air content in the concrete resulted in different strengths for each mix, rather than consistent strengths across all mixes. Therefore, the strength effect related to the degree of freeze–thaw impact cannot be ignored. Future research should focus on the effects of freeze–thaw cycles on RC beams with different air contents but the same compressive strength. In addition, since the existing freeze–thaw method only applied the A-type (*A* test), further research on the B-type freeze–thaw test is also necessary.

Acknowledgements
This research was supported by Basic Science Research Program through the National Research Foundation of Korea (NRF) funded by the Ministry of Education (RS-2023-00248882)

Author contributions
SK contributed to the writing—original draft and formal analysis. YL contributed to data curation and investigation. JK contributed to supervision

and project administration. DH contributed to the supervision, and writing—review and editing. All authors read and approved the final manuscript.

Funding
This research was supported by Basic Science Research Program through the National Research Foundation of Korea (NRF) funded by the Ministry of Education (RS-2023-00248882).

Availability of data and materials
All data is provided in full in the results of this paper.

Declarations

Ethics approval and consent to participate
Not applicable.

Consent for publication
Not applicable.

Competing interests
The authors declare that they have no known competing financial interests or personal relationships that could have appeared to influence the work reported in this paper.

Received: 26 June 2024 Accepted: 3 November 2024
Published online: 11 February 2025

References

ASTM C143 /C143M-20. (2020). Standard test method for slump of hydraulic-cement concrete, West Conshohocken, PA: American Society for Testing and Materials.
ASTM C150-07. (2022). Standard specification for portland cement, West Conshohocken, PA: American Society for Testing and Materials.
ASTM C231/C231M-22. (2022). Standard test method for air content of freshly mixed concrete by the pressure method, West Conshohocken, PA: American Society for Testing and Materials.
ASTM C33/C33M-23. (2023). Standard specification for concrete aggregates, West Conshohocken, PA: American Society for Testing and Materials.
ASTM C666/C666M-15. (2016). Standard test method for resistance of concrete to rapid freezing and thawing, West Conshohocken: American Society for Testing and Materials.
ASTM C94/C94M-23. (2023). Standard specification for ready-mixed concrete, West Conshohocken, PA: American Society for Testing and Materials.
Chen, D., Guo, W., Kang, J., & Shi, J. (2023). Experimental and modelling investigation on chloride transport and flexural behaviour of RC beams subjected to simultaneous deteriorating factors of carbonation, FT cycles and multi-type sustained stress. *Construction and Building Materials, 397*, 132305. https://doi.org/10.1016/j.conbuildmat.2023.132305
Cordon, W. A. (1967), Freezing and thawing of concrete, mechanisms and control, ACI Monograph Nr 3, Farmington Hills, MI, American Concrete Institute, 1967.
Dahmani, L., Khenane, A., & Kaci, S. (2007). Behavior of the rein-forced concrete at cryogenic temperatures. *Cryogenics, 47*(9/10), 517–525.
Fülöp, L., Ferreira, M., Bohner, E., Valokoski, J., Vuotari, J., & Tirkkonen, T. (2022). Inspection of bridges for effects of air-entrainment on the porosity and compressive strength of concretes. *Case Studies in Construction Materials, 17*, e01211. https://doi.org/10.1016/j.cscm.2022.e01211
Gong, F. Y., & Maekawa, K. (2018). Multi-scale simulation of freeze-thaw damage to RC column and its restoring force characteristics. *Engineering Structures, 156*, 522–536.
Holan, J., Novák, J., Müller, P., & Štefan, R. (2020). Experimental investigation of the compressive strength of normal-strength air-entrained concrete at high temperatures. *Construction and Building Materials, 248*, 118662. https://doi.org/10.1016/j.conbuildmat.2020.118662
Jang, G. S., Yun, H. D., Kim, S. W., Park, W. S., & Choi, K. B. (2009). Flexural behavior of reinforced concrete beams exposed to freeze-thawing environments. *Journal of the Korea Institute for Structural Maintenance Inspection, 13*(6), 126–134.
Jiang, Z. W., He, B., Zhu, X. P., Ren, Q., & Zhang, Y. (2020). State-of-the-art review on properties evolution and deterioration mechanism of concrete at cryogenic temperature. *Construction and Building Materials, 257*, 119456.
Kim, J. S. (2023). Flexural behavior of RC beam according to the change in adhesion between rebar and concrete due to complex deterioration. *Journal of Korean Society Advanced Composite Structures, 14*(5), 17–22. https://doi.org/10.11004/kosacs.2023.14.5.017
Kim, J. S., Jung, W. Y., & Kwon, M. H. (2013). Performance evaluation of the post-installed anchor for sign structure in South Korea. *Construction and Building Materials, 44*, 496–506.
Kim, S. W., Lee, D. J., Kim, K. M., & Kim, J. S. (2020). Evaluation of behavior characteristics of reinforced concrete beam structures by freeze-thawing. *Journal of Korean Society Advanced Composite Structures., 11*(2), 39–45. https://doi.org/10.11004/kosacs.2020.11.2.039
Kim, S. W., Lee, D. J., Kim, K. M., & Kim, J. S. (2021). An experimental study on the performance of RC beam according to the rapid freezing and thawing test method in the air. *Journal of Korea Institute for Structural Maintenance and Inspection, 25*(4), 46–55. https://doi.org/10.11112/jksmi.2021.25.4.46
KS F 2405. (2022). Test method for compressive strength of concrete, Korean Agency for Technology and Standards (KS), Seoul, Korea.
KS F 2527. (2022). Aggregates for concrete, Korean Agency for Technology and Standards (KS), Seoul, Korea.
Kwon, G. B., Lee, D. J., Kim, K. M., Kwon, M. H., & Kim, J. S. (2020). A study on adhesion behavior of CFRP composite plate attached on the RC beams by freezing and thawing. *Journal of Korean Society Advanced Composite Structures., 11*(2), 1–6. https://doi.org/10.11004/kosacs.2020.11.2.001
Kwon, M. H., Kim, J. S., Jung, W. Y., & Kwon, S. W. (2013). An performance evaluation of the post-installed anchor system according to the freezing and thawing of concrete and the corrosion of anchor. *Journal of Korea Institute for Structural Maintance and Inspection, 17*(5), 31–39. https://doi.org/10.11004/kosacs.2020.11.2.001
Luo, Y. J., Cui, W., & Song, H. F. (2020). Poromechanical microplane model with thermodynamics for deterioration of concrete subjected to freeze-thaw cycles. *Journal of Materials in Civil Engineering, 32*(11), 04020338.
Maiti, S. C., Agarwal, R. K., & Kumar, R. (2006). Concrete mix proportioning. *The Indian Concrete Journal, 80*(12), 23–26.
Mehta, P. K. (1991) Concrete durability - fifty years progress, In: Proc. of 2nd Inter Conf. On Concrete Durability, ACISP. J., pp. 1–31.
Neville, A. (2001). Consideration of durability of concrete structures: Past, present and future. *Materials and Structures, 34*(3), 114–118.
Oh, B. H., Han, S. H., Park, S. H., & Lee, Y. H. (1993). Experimental study of freezing and thawing characteristics of concrete influenced by air content and water cement ratio. *Korean Concrete Institute Conference Proceedings, 5*(2), 91–96.
Park, G. M., Park, S. H., Chu, Y. K., & Lee, S. T. (2020). Evaluation of the resistance of freezing and thawing according to the amount of air in concrete. *Korean Concrete Institute Conference Proceedings, 32*(2), 257–258.
Powers, T. C. (1945). A working hypothesis for further studies of frost resistance. *Journal of American Concrete Institute., 16*(4), 245–272.
Powers, T. C., & Helmuth, R. A. (1953). Theory of volume change in hardened Portland cement paste during freezing. *Highway Research Board Proc., 32*, 285–297.
Rong, X. L., Li, L., Huang, W. Y., Dong, L. G., Zheng, S. S., Wang, F., Lu, D., & Wang, J. Y. (2023b). Experimental investigation of the seismic resistance of RC beam-column connections after freeze-thaw cycle treatment. *Engineering Structures., 290*, 116330. https://doi.org/10.1016/j.engstruct.2023.116330
Rong, X. L., Li, L., Zheng, S. S., Wang, F., Huang, W. Y., Zhang, Y. X., & Lu, D. (2023a). Freeze-thaw damage model for concrete considering a nonuniform temperature field. *Journal of Building Engineering., 72*, 106747. https://doi.org/10.1016/j.jobe.2023.106747
Rustamov, S., Kim, S. W., Kwon, M. H., & Kim, J. S. (2021). Mechanical behavior of fiber-reinforced lightweight concrete subjected to repeated freezing and thawing. *Construction and Building Materials, 273*, 121710. https://doi.org/10.1016/j.conbuildmat.2020.121710
Salem, M. A. A., & Pandey, R. K. (2015). Effect of air entrainment on compressive strength. *Density, and Ingredients of Concrete, International Journal of Modern Engineering Research, 5*(1), 77–81.

Shang, H., Song, Y., & Ou, J. (2009). Behavior of air-entrained concrete after freeze-thaw cycles. *Acta Mechanica Solida Sinica, 22*(3), 261–266.
Shi, X., Xie, N., Fortune, K., & Gong, J. (2012). Durability of steel reinforced concrete in chloride environments: An overview. *Construction and Building Materials, 30*, 125–138. https://doi.org/10.1016/j.conbuildmat.2011.12.038
Shin, J. H., Choi, H. G., Hong, J. H., Beak, H. S., Seo, K. H., & Park, M. Y. (2019). A study on basic properties of concrete using carbon nanomaterials. *Korean Concrete Institute Conference Proceedings, 31*(2), 561–562.
Sun, Z., Wan, Z., & Sachs, S. G. (2023). Compatibility of carbon nanotube in concrete with air entrainer and superplasticizer. *Construction and Building Materials, 364*, 129944. https://doi.org/10.1016/j.conbuildmat.2022.129944
Wang, J. Y., Rong, X. L., Zheng, S. S., Zhang, Y. X., Dai, K. Y., Dong, L. G., & Wang, Z. S. (2022). Cyclic behavior of RC beams under artificial climate rapid freeze-thaw environment: A further research. *Case Studies in Construction Materials, 17*, e01589. https://doi.org/10.1016/j.cscm.2022.e01589
Yang, S., Chen, X., Han, M., & Song, J. (2022). Effect of sulfate attack, drying-wetting cycles and freezing-thawing cycles on reinforced concrete columns under eccentric loads. *Structures, 45*, 1864–1877. https://doi.org/10.1016/j.istruc.2022.10.011
Yin, T., Zhu, W., Xu, B., Zhang, Y., & Gao, W. (2023). Deterioration law of flexural performance of RC beams with initial cracks under alternating action of salt freeze-thaw cycles and fatigue. *Construction and Building Materials, 409*, 134052. https://doi.org/10.1016/j.conbuildmat.2023.134052
Zhang, Y., Zheng, S., Li, L., Dong, L., Ji, J., & Ruan, S. (2021). Modeling the lateral behavior of freeze-thaw damaged reinforced concrete columns including reinforcement slip and shear effects. *Engineering Structures, 237*, 112168. https://doi.org/10.1016/j.engstruct.2021.112168
Zhao, P., Xu, G., Wang, Q., & Wen, C. (2021). Impact of sustained load on damage characteristics of reinforced concrete beams under the combined action of salt freeze-thaw cycles and corrosion. *Construction and Building Materials, 273*, 121744. https://doi.org/10.1016/j.conbuildmat.2020.121744

Publisher's Note

Sangwoo Kim Ph.D. candidate, Dept. of Civil Engineering, Gyeongsang National University, Jinju 52828, Republic of Korea

Yujeong Lee Ph.D. candidate, Dept. of Architectural Engineering, Gyeongsang National University, Jinju 52828, Republic of Korea

Jinsup Kim Associate Professor, Dept. of Civil Engineering, Gyeongsang National University, Jinju 52828, Republic of Korea,

Dongyeop Han Associate Professor, Dept. of Architectural Engineering, Gyeongsang National University, Jinju 52828, Republic of Korea.